Pressure-induced commensurate phase with potential giant polarization in YMn_2O_5

M. Deutsch, T.C. Hansen, M. T. Fernández-Díaz, A. Forget, D. Colson, F. Porcher, I. Mirebeau

PHYSICAL REVIEW B **92**, 060410(R) (2015)

Pressure-induced commensurate phase with potential giant polarization in YMn_2O_5

M. Deutsch,[1,2] T. C. Hansen,[3] M. T. Fernandez-Diaz,[3] A. Forget,[4] D. Colson,[4] F. Porcher,[1] and I. Mirebeau[1,*]

[1]*CEA, Centre de Saclay, DSM/IRAMIS/Laboratoire Léon Brillouin, F-91191 Gif-sur-Yvette, France*

[2]*Synchrotron SOLEIL, L'Orme des Merisiers, Saint-Aubin, F-91192 Gif-sur-Yvette, France*

[3]*Institut Laue Langevin, 6 rue Jules Horowitz, BP 156, F-38042 Grenoble, France*

[4]*CEA, Centre de Saclay, DSM/IRAMIS/SPEC, F-91191 Gif-sur-Yvette, France*

(Received 10 June 2015; published 21 August 2015)

We have studied multiferroic YMn_2O_5 by high-pressure neutron diffraction in a large pressure range from 0.5 to 6.3 GPa. We observe a pressure-induced commensurate (PCM) phase with a propagation vector $(\frac{1}{2}0\frac{1}{2})$ that is different from those observed at ambient pressure. It coexists with the ambient pressure phases up to the highest pressure, with an increased contribution as the pressure increases. The PCM phase, which is likely generic in the RMn_2O_5 family, should be taken into account to understand the strong variation of the electric polarization under pressure.

DOI: 10.1103/PhysRevB.92.060410 PACS number(s): 75.25.−j, 75.85.+t

Multiferroic materials, which were discovered in Russia in the 1970's, have attracted a renewed interest for the past decade. The coupling between magnetic and electric orders makes them promising for industrial applications, by manipulating the magnetization via an electric field or the electric polarization via a magnetic field. The strongest effects have been found in the magnetically induced ferroelectrics $RMnO_3$ and RMn_2O_5 (where R is a rare earth, Bi, or Y ion), which show complex magnetic structures upon varying the temperature due to the presence of frustrated interactions. The coupling mechanism underlying these effects is a central issue. In orthorhombic $RMnO_3$ and especially in $TbMnO_3$, it was ascribed to the inverse Dzyaloshinskii-Moriya (DM) effect [1], assuming that the cycloidal order breaks the inversion symmetry by inducing atomic displacements to minimize the DM energy. This mechanism yields an electric polarization proportional to the vector product of neighboring spins ($P \propto \mathbf{S_i} \times \mathbf{S_j}$). In contrast, in RMn_2O_5 where the electric polarization appears together with an almost collinear magnetic order, another mechanism based on exchange striction was proposed [2–4], where the polarization is proportional to the scalar product between neighboring spins ($P \propto \mathbf{S_i} \cdot \mathbf{S_j}$). A microscopic model assuming isotropic Heisenberg exchange and magnetostrictive spin coupling explains several features of the RMn_2O_5, such as the electromagnon [5,6]. It is, however, likely that in RMn_2O_5 several mechanisms are at play, and either one or the other dominates, depending on the temperature range considered [7–10].

In the RMn_2O_5 family, YMn_2O_5 has been widely studied [7–9,11,12], since the nonmagnetic Y allows one to test coupling schemes involving interactions solely between Mn ions. It exhibits a sequence of magnetic phase transitions similar to the other members (Fig. 1), with a transition at T_{N1} (44 K) from the paramagnetic state to a high temperature incommensurate (HT-INC) magnetic structure, followed by a transition into a commensurate (CM) structure at T_{C1} (38 K), then by a reentrant transition into a low temperature incommensurate (LT-INC) phase at T_{C2} (20 K). The magnetic phases show different dielectric properties. The HT-INC phase is paraelectric, the CM and LT-INC phases are both ferroelectric, but the polarization changes sign at T_{C2} and maintains a lower value in the LT-INC phase.

Applying pressure is a suitable way to investigate the magnetoelectric coupling in multiferroics [13], since changing the interatomic distances influences the energy balance between the frustrated magnetic interactions, which therefore changes the magnetic structure. High-pressure neutron diffraction allows one to investigate such changes at a microscopic level, but rather few experiments have been performed so far [14–20]. In $TbMnO_3$ an applied pressure stabilizes an E-type CM magnetic phase, as observed in $HoMnO_3$, and modifies the INC phase by inducing a phase shift of the magnetic order between neighboring Mn chains [21]. These changes result in a giant ferroelectric polarization [22]. In YMn_2O_5 (and in RMn_2O_5 with R = Tb,Ho,Dy), a pressure-induced polarization reversal (growth) has been observed [12,23], but the underlying changes of the magnetic structure have yet to be studied.

In this Rapid Communication, we report the study of YMn_2O_5 by high-pressure powder neutron diffraction in a large pressure range (0–6.3 GPa), down to low temperatures (1.5 K), and by combining various pressure setups. We have observed a pressure-induced commensurate phase (called PCM in the following), with a propagation vector different from that of the CM phase stabilized at ambient pressure. We followed its growth with increasing pressure, and provide a semiquantitative description of the pressure-induced phase separation. Our results imply that the polarization reversal with pressure should be reinterpreted. As a possible consequence, within the exchange striction model previously assumed for the LT-INC and CM phases, our PCM phase should carry a giant polarization.

The pure polycrystalline YMn_2O_5 compound was prepared by a solid state reaction from a stoichiometric mixture of Y_2O_3 (99.99%) and Mn_2O_3 (99%). The powder was heated for 18 h, for four times from 1050 to 1085 °C under oxygen flux, cooled down to room temperature, and reground after each calcination. It was measured at ambient pressure and up to 2.9 GPa on the powder diffractometer G6.1 of the Laboratoire Léon Brillouin (LLB) with an incident neutron wavelength of 4.74(2) Å, using focusing devices in the high-pressure version.

*isabelle.mirebeau@cea.fr

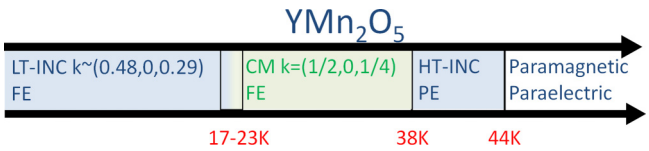

FIG. 1. (Color online) General phase diagram of YMn_2O_5. HT-INC: high temperature incommensurate magnetic structure; CM: commensurate magnetic structure; LT-INC: low temperature incommensurate magnetic structure; PE: paraelectric; FE: ferroelectric.

We used a Cu-Be piston cylinder cell at pressures up to 1.2 GPa, and a Kurchatov-LLB pressure cell with sapphire anvils up to 2.9 GPa. High-pressure patterns were collected at 4.2 and 6.3 GPa on the high flux diffractometer D20 of the Institut Laue Langevin (ILL) using a neutron wavelength of 2.42 Å and a Paris-Edinburgh pressure cell. See the Supplemental Material for details about the experimental conditions [24].

Ambient pressure patterns are shown in Fig. 2 at two typical temperatures in the CM and LT-INC phases. The insets show the magnetic patterns obtained by subtracting a pattern in the paramagnetic region. Good refinements are obtained with the models of Refs. [11,25]. According to these models, in the CM phase of the propagation vector $(\frac{1}{2}0\frac{1}{4})$, the Mn moments are almost collinear and make zigzag antiferromagnetic (AF) chains, with a weak component along c, modulated in phase quadrature

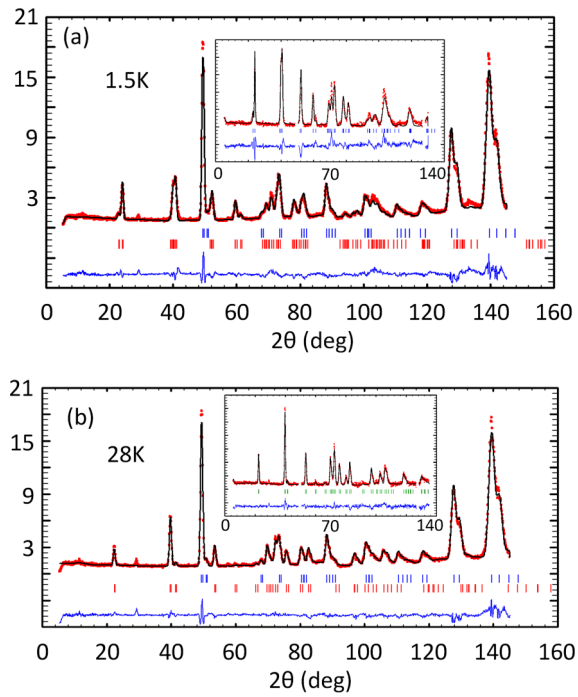

FIG. 2. (Color online) Refined diffraction patterns at ambient pressure. (a) $T = 1.5$ K; (b) $T = 28$ K. The patterns were refined with (a) LT-INC and (b) CM phases, according to Ref. [11] for LT-INC and Ref. [25] for CM. The solid black line is a FULLPROF refinement; tick marks show the Bragg peak positions for the structural (blue) and magnetic (red) phases. The solid blue line is the difference between the calculated and measured patterns. Refined magnetic patterns obtained by subtracting a pattern at 50 K are shown in the insets. The R values are $R_N = 5.7\%$ and $R_{M(\mathrm{INC})} = 15.8\%$ at 1.5 K and $R_N = 6.2\%$ and $R_{M(\mathrm{CM})} = 9.9\%$ at 28 K.

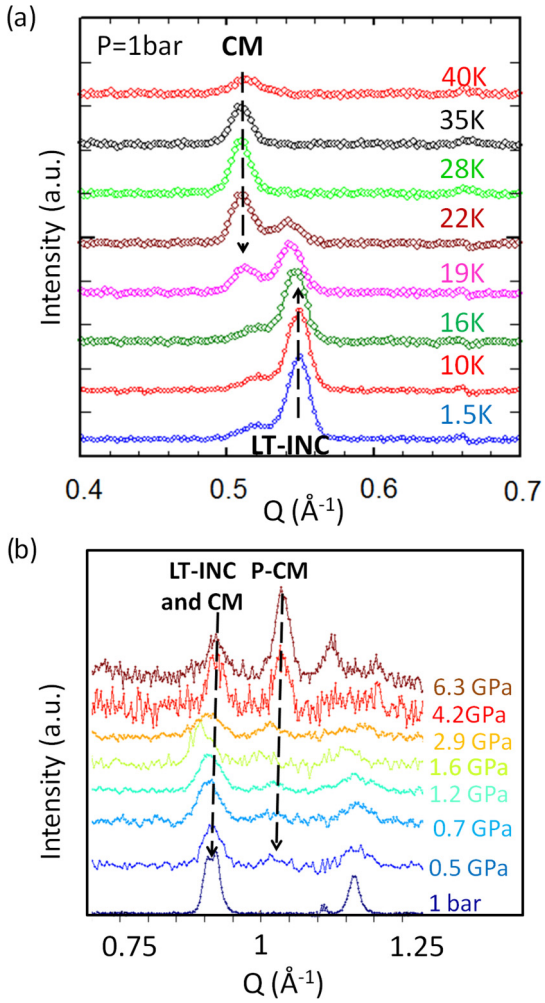

FIG. 3. (Color online) YMn_2O_5 diffraction patterns, focusing on the Q range of interest. (a) Temperature evolution at ambient pressure (1 bar). The CM and LT-INC phases coexist between 17 and 23 K. (b) Pressure evolution of the magnetic patterns at 1.5 K. A pattern at 50 K is subtracted. Patterns measured on G6.1 (up to 2.9 GPa) and D20 (4.2 and 6.3 GPa) have been scaled to the intensity of the nuclear peaks to be compared. LT-INC, CM, and PCM are the incommensurate, commensurate, and pressure-induced commensurate phases, respectively. The peak at 1.2 $Å^{-1}$ and 6.3 GPa, situated at a nuclear peak position, is attributed to an imperfect subtraction.

with the *ab* component. In the LT-INC phase of the propagation vector (0.48 0 0.29), spin reorientation occurs, together with the formation of a long-period cycloid along a. The values and orientations of the Mn moments are very close to those found in Ref. [11]. The CM and LT-INC coexist in the temperature range 17–23 K [see Fig. 3(a)], and their relative fraction changes with temperature, as expected in a first-order transition.

As our main result, under pressure we observe a commensurate phase (PCM) that is different from the CM phase observed at ambient pressure. Its existence is clearly shown in Fig. 3(b) by the onset of a magnetic peak at $Q \sim 1$ $Å^{-1}$ which cannot be indexed with the **k** vectors at ambient pressure. The pressure-induced magnetic phase is observed at all temperatures below T_N and at all pressures in the

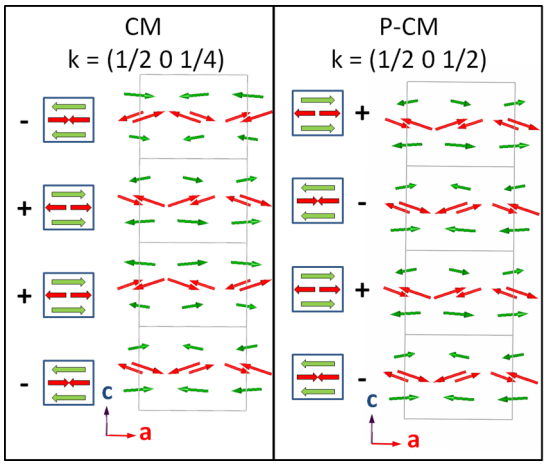

FIG. 4. (Color online) Schematic drawing of the Mn moment orientations in the CM and PCM phases in the *ac* plane; green and red arrows correspond to Mn^{4+} and Mn^{3+} moments, respectively; a simplified drawing of the stacking sequence of magnetic moments along the *c* axis is also drawn.

range 0.5–6.3 GPa. It coexists with the LT-INC and/or CM phases observed at ambient pressure. With increasing pressure, the amount of PCM increases whereas those of the ambient pressure phases decrease, as shown by the opposite variations of the peak intensities with pressure. The peak at $Q \sim 1$ Å^{-1} relative to the PCM phase is indexed by the propagation vector $\mathbf{k} = (\frac{1}{2}0\frac{1}{2})$. Patterns measured on D20 with a shorter wavelength confirm the value of the propagation vector by showing other related peaks of weaker intensity. They also allow us to analyze the PCM phase in a pressure range where it is dominant.

To analyze the pressure effect we focus on the lowest temperature ($T = 1.5$ K for G6.1 and 5 K for D20) where the PCM phase is better separated. We refine the high-pressure patterns by assuming that (i) the magnetic structures of the LT-INC and CM phases are unchanged under pressure, and (ii) the PCM magnetic structure is similar to the CM one, namely, the spin arrangement in a given *ab* plane is the same, but the stacking of *ab* planes along *c* changes from $++--$ ($k_z = \frac{1}{4}$) to $+-+-$ ($k_z = \frac{1}{2}$) under pressure, as shown by the schematic drawing of Fig. 4. The above constraints are imposed to limit the number of refined parameters, since the PCM phase could not be observed as a single phase, regardless of the temperature or pressure. The lower statistics of the high-pressure patterns and the peak overlap from the different phases prevent a full characterization. Within these assumptions, we obtained satisfactory refinements of the pressure patterns by refining only the scale factors of the LT-INC, CM, and PCM phases, which yield their relative amounts. Typical refinements are shown in Fig. 5. In the pressure range of 0.5–2.9 GPa, the best fit is obtained by assuming that the three phases coexist. At high pressures (4.2 and 6.3 GPa) the best fit is obtained with the CM and PCM phases only, although a small amount of the LT-INC phase could not be discarded, being difficult to separate from the CM phase on the D20 patterns. In Fig. 6(a), we show the phase fractions deduced from these refinements. As

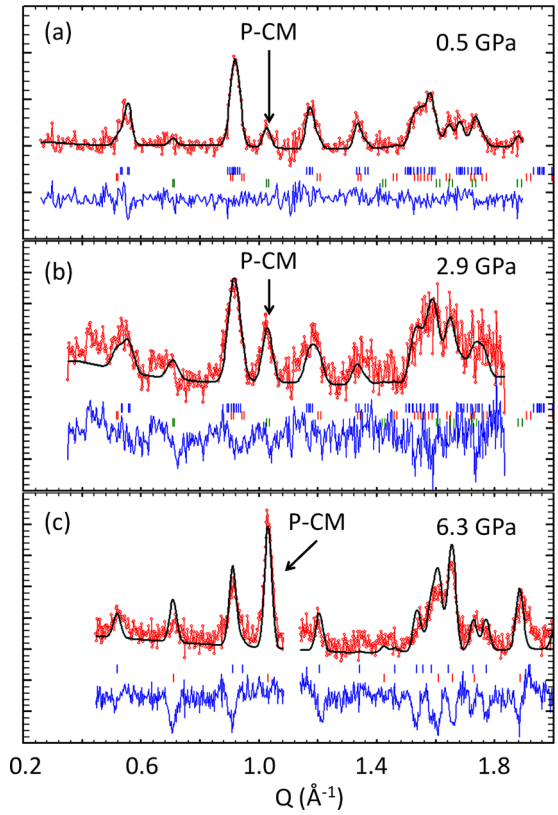

FIG. 5. (Color online) YMn_2O_5 magnetic patterns (a pattern in the paramagnetic phase was subtracted) measured at (a) 0.5 GPa on the G6.1 spectrometer and fitted with the coexistence of three phases, (b) 2.9 GPa on the G6.1 spectrometer and fitted with the coexistence of three phases, and (c) 6.3 GPa on the D20 spectrometer with the coexistence of two phases. Red dots are experimental data, and the solid black line is a FULLPROF [26] refinement; tick marks indicate the Bragg peak positions for the structural and magnetic phases. The solid blue line is the difference between the calculated and measured patterns. The *R* values are $R_{M(\mathrm{INC})} = 12.97\%$, $R_{M(\mathrm{CM})} = 16.54\%$, and $R_{M(\mathrm{PCM})} = 15.98\%$ at 1.5 K and 0.5 GPa, and $R_{M(\mathrm{INC})} = 24.09\%$, $R_{M(\mathrm{CM})} = 31.42\%$, and $R_{M(\mathrm{PCM})} = 19.55\%$ at 1.5 K and 2.9 GPa.

pressure increases, the CM and PCM phases slowly grow at the expense of the LT-INC.

Another evaluation of the pressure-induced phase separation can be obtained, without any *a priori* model for the magnetic structures, by plotting the area of selected magnetic peaks versus pressure, scaled by the area of a nuclear peak. We consider the peaks of Fig. 3(b), namely, the $(\frac{1}{2}1\frac{1}{2})$ peak of the PCM phase at $Q = 1$ Å and the peak around $Q = 0.9$ Å resulting from the overlap of the $(\frac{1}{2}1\frac{1}{4})$ and (0.48 1 0.29) [and quasiequivalent satellite (0.48 0 0.71) . . .] peaks of the CM and LT-INC phases, respectively. Their total area is constant with pressure, which justifies this analysis. The corresponding phase fractions [see Fig. 6(b)] show the same tendency as above. At 6.3 GPa, the amount of the PCM phase reaches 30% and 60% for the model and model-free evaluations, respectively. The extrapolated pressures where this phase would stand alone are situated in the range 9–16 GPa. Therefore, our main conclusions concerning the pressure-induced phases are robust, regardless of the detailed nature of their magnetic structures.

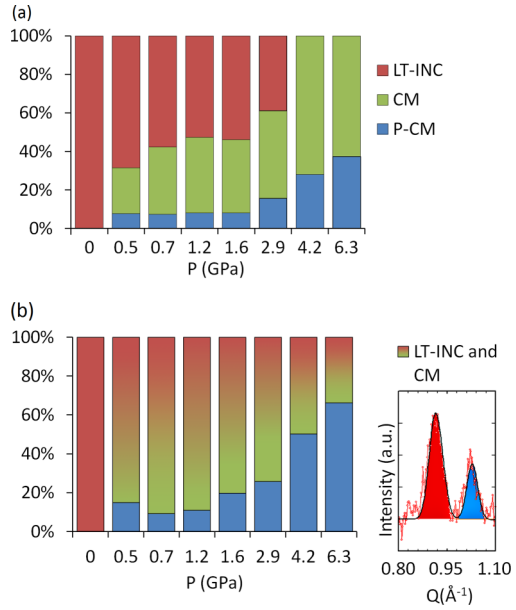

FIG. 6. (Color online) Pressure-induced magnetic phase separation in YMn_2O_5 at low temperature ($\leqslant 5$ K). The relative amounts of the LT-INC, CM, and PCM phases are deduced (a) from the refined diffraction patterns and (b) from the intensity of selected peaks, plotted on the right.

The onset of the PCM phase should have important consequences on the electric polarization. At ambient pressure, according to the exchange striction model in Ref. [27], the net electric polarization along the b axis is calculated as

$$P^{\mathrm{INC}} = 4C\vec{S}_3 \cdot \vec{S}_4 \cos\left[2\pi\left(\tfrac{1}{4}+\delta_z\right)z'\right]\cos\left[2\pi\delta_x\left(\tfrac{1}{2}-x\right)\right] \times \cos(\epsilon)\sin(\varphi), \quad (1)$$

where $\vec{S}_3$ and $\vec{S}_4$ are the magnetic moments of Mn^{3+} and Mn^{4+}, respectively, and C is the magnetoelastic coupling constant. The propagation vector of the LT-INC phase is $k = (\frac{1}{2}+\delta_x, 0, \frac{1}{4}+\delta_z)$ and z' is the fractional coordinate $z' = z - \frac{1}{2}$. ϕ is the global phase shift between the wave modulations of adjacent zigzag chains along b; the Mn moments also follow a sinusoidal modulation along c with a phase shift ϵ. The polarization in the CM and PCM commensurate phase is obtained by setting δ_x, δ_z, the phase shift ϵ to zero, and the global phase shift $\varphi = \frac{\pi}{2}$. For the LT-INC, CM, and PCM phases, this yields a polarization of

$$P = 4C\alpha\vec{S}_3 \cdot \vec{S}_4, \quad (2)$$

with $\alpha \simeq -0.2$, 0.9, and 0.7 for the LT-INC, CM, and PCM phases, respectively. At ambient pressure, this expression well accounts for the strong temperature dependence of the polarization which reverses its sign at T_{C2}, changing from a high positive value in the CM phase (around 100 nC cm^{-2}) to a lower negative value (-20 nC cm^{-2}) in the LT-INC phase. Under a pressure of 1.6 GPa, the polarization recovers a positive value of 150 nC cm^{-2}, close to the value in the CM phase [12]. This recovery was naturally attributed to the growth of the CM phase under pressure, assuming that this phase dominates at 1.6 GPa. Our measurements show that the situation is more complicated, since, with our assumption, three phases actually coexist at 1.6 GPa, with relative amounts around 54%, 38%, and 8% for the LT-INC, CM, and PCM phases, respectively. Assuming that the polarizations of the LT-INC and CM phases are the same as those of ambient pressure, the PCM phase should carry a giant polarization of about 1.4 μC cm^{-2} at 1.6 GPa to compensate for the negative contribution of the LT-INC phase. In such a case, one should expect a further increase of the polarization with increasing pressure above 1.6 GPa, reaching very high values at high pressures when this phase dominates (960 nC cm^{-2} at 6.3 GPa, for instance). Keeping the exchange striction scenario, the polarization of the PCM phase should remain high (above 1 μC cm^{-2}) even if the phase shifts between the Mn moment in the zigzag chains switch the sign of polarization in the LT-INC phase under pressure. Alternatively, another mechanism such as that predicted by the inverse DM model could be at play, with a change of balance between the two mechanisms yielding a complete redistribution of the polarization under pressure. Polarization measurements under high pressures would be useful to check these scenarios.

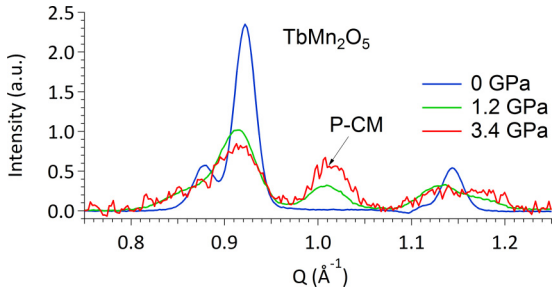

FIG. 7. (Color online) $TbMn_2O_5$: Magnetic patterns at 1.5 K showing the onset of a pressure-induced commensurate phase. A pattern at 56 K is subtracted.

In conclusion, we have observed a pressure-induced commensurate phase in YMn_2O_5, and characterized by a propagation vector $(\frac{1}{2}0\frac{1}{2})$ that is different from that of the ambient pressure CM phase. We have given a semiquantitative description of the pressure-induced phase separation. Within the exchange striction model, our results suggest that this phase carries a giant electric polarization. Another explanation could be a complete redistribution of the polarization under pressure due to a change of balance between the two previously invoked mechanisms (exchange striction and inverse DM). Our preliminary measurements show that this PCM phase also exists in $TbMn_2O_5$ (see Fig. 7), suggesting that it could be a generic feature of the RMn_2O_5 family. It should thus be taken into account to understand the surprising evolution of the polarization with temperature and pressure [23].

We are deeply grateful to O. L. Makarova for her valuable help in the high-pressure experiments. We are thankful to S. Petit, L. Chapon, P. Foury, and V. Baledent for useful discussions. We also thank S. Kichanov for his help during the initial measurements at LLB and B. Annighoefer for his help with the pressure cell. The post-doctoral training of M.D. was funded by the French Project ANR (DYMAGE) and Triangle de la Physique, Contract 2012-042T-Helix. A public

grant from the "Laboratoire d'Excellence Physics Atom Light Mater" (Labex PALM) was overseen by the French National Research Agency (ANR) as part of the "Investissements d'Avenir" program (Grant No. ANR-10-LABX-0039-PALM).

[1] H. Katsura, N. Nagaosa, and A. V. Balatsky, Phys. Rev. Lett. **95**, 057205 (2005).
[2] S.-W. Cheong and M. Mostovoy, Nat. Mater. **6**, 13 (2007).
[3] L. C. Chapon, G. R. Blake, M. J. Gutmann, S. Park, N. Hur, P. G. Radaelli, and S.-W. Cheong, Phys. Rev. Lett. **93**, 177402 (2004).
[4] J. J. Betouras, G. Giovannetti, and J. van den Brink, Phys. Rev. Lett. **98**, 257602 (2007).
[5] A. B. Sushkov, M. Mostovoy, R. V. Aguilar, S.-W. Cheong, and H. D. Drew, J. Phys.: Condens. Matter **20**, 434210 (2008).
[6] J.-H. Kim, M. A. van der Vegte, A. Scaramucci, S. Artyukhin, J.-H. Chung, S. Park, S.-W. Cheong, M. Mostovoy, and S.-H. Lee, Phys. Rev. Lett. **107**, 097401 (2011).
[7] J.-H. Kim *et al.*, Phys. Rev. B **78**, 245115 (2008).
[8] S. Wakimoto, H. Kimura, Y. Sakamoto, M. Fukunaga, Y. Noda, M. Takeda, and K. Kakurai, Phys. Rev. B **88**, 140403 (2013).
[9] S. Partzsch, S. B. Wilkins, J. P. Hill, E. Schierle, E. Weschke, D. Souptel, B. Büchner, and J. Geck, Phys. Rev. Lett. **107**, 057201 (2011).
[10] V. Balédent, S. Chattopadhyay, P. Fertey, M. B. Lepetit, M. Greenblatt, B. Wanklyn, F. O. Saouma, J. I. Jang, and P. Foury-Leylekian, Phys. Rev. Lett. **114**, 117601 (2015).
[11] P. G. Radaelli, C. Vecchini, L. C. Chapon, P. J. Brown, S. Park, and S.-W. Cheong, Phys. Rev. B **79**, 020404 (2009).
[12] R. P. Chaudhury, C. R. dela Cruz, B. Lorenz, Y. Sun, C.-W. Chu, S. Park, and S.-W. Cheong, Phys. Rev. B **77**, 220104(R) (2008).
[13] E. Gilioli and L. Ehm, IUCrJ **1**, 590 (2014).
[14] D. P. Kozlenko, I. Mirebeau, J.-G. Park, I. N. Goncharenko, S. Lee, J. Park, and B. N. Savenko, Phys. Rev. B **78**, 054401 (2008).
[15] H. Kimura, K. Nishihata, Y. Noda, N. Aso, K. Matsubayashi, Y. Uwatoko, and T. Fujiwara, J. Phys. Soc. Jpn. **77**, 063704 (2008).
[16] D. P. Kozlenko, A. A. Belik, S. E. Kichanov, I. Mirebeau, D. V. Sheptyakov, Th. Strässle, O. L. Makarova, A. V. Belushkin, B. N. Savenko, and E. Takayama-Muromachi, Phys. Rev. B **82**, 014401 (2010).
[17] D. P. Kozlenko, S. E. Kichanov, E. V. Lukin, S. Lee, J.-G. Park, and B. N. Savenko, High Press. Res. **30**, 252 (2010).
[18] D. P. Kozlenko, A. A. Belik, A. V. Belushkin, E. V. Lukin, W. G. Marshall, B. N. Savenko, and E. Takayama-Muromachi, Phys. Rev. B **84**, 094108 (2011).
[19] O. L. Makarova *et al.*, Appl. Phys. Lett. **103**, 082907 (2013).
[20] N. Terada, D. D. Khalyavin, P. Manuel, T. Osakabe, P. G. Radaelli, and H. Kitazawa, Phys. Rev. B **89**, 220403 (2014).
[21] O. L. Makarova, I. Mirebeau, S. E. Kichanov, J. Rodriguez-Carvajal, and A. Forget, Phys. Rev. B **84**, 020408 (2011).
[22] T. Aoyama, A. Iyama, K. Shimizu, and T. Kimura, Phys. Rev. B **91**, 081107 (2015).
[23] C. R. dela Cruz, B. Lorenz, Y. Y. Sun, Y. Wang, S. Park, S.-W. Cheong, M. M. Gospodinov, and C. W. Chu, Phys. Rev. B **76**, 174106 (2007).
[24] See Supplemental Material at http://link.aps.org/supplemental/10.1103/PhysRevB.92.060410 for details about the experimental conditions.
[25] C. Vecchini, L. C. Chapon, P. J. Brown, T. Chatterji, S. Park, S.-W. Cheong, and P. G. Radaelli, Phys. Rev. B **77**, 134434 (2008).
[26] J. Rodriguez-Carvajal, Physica B (Amsterdam) **192**, 55 (1993).
[27] L. C. Chapon, P. G. Radaelli, G. R. Blake, S. Park, and S.-W. Cheong, Phys. Rev. Lett. **96**, 097601 (2006).